Opt Quant Electron (2015) 47:2993–3007
DOI 10.1007/s11082-015-0186-2

Analysis of ultra-high birefringent fully-anisotropic photonic crystal fiber

Rasha A. Hussein[1,2] · Mohamed Farhat O. Hameed[3,4] · Jala El-Azab[1] · Wessameldin S. Abdelaziz[1] · S. S. A. Obayya[3]

Received: 2 March 2015 / Accepted: 4 May 2015 / Published online: 20 May 2015

Abstract Highly birefringent photonic crystal fiber (PCF) is proposed and analyzed using full vectorial finite element method. The reported design has a central large core filled with nematic liquid crystal (NLC) which provides tunability with the external electric field and temperature. In addition, the full permittivity tensor of the NLC material is taken into account when we study the modal properties of the proposed PCF. The effects of the geometrical parameters, rotation angle of the director of the NLC, and temperature on the modal properties of the reported design are investigated. The suggested design offers high birefringence of 0.191 at the operating wavelength of 1.55 μm with NLC diameter of 3.4 μm with low losses of the two polarized modes. As the NLC diameter decreases to 1.0 μm, high birefringence of 0.08 is obtained with single mode NLC PCF design, which is significantly large birefringence to maintain polarization state.

Keywords Photonic crystal fibers · Nematic liquid crystal · Finite element method · Birefringence

✉ S. S. A. Obayya
sobayya@zewailcity.edu.eg

Rasha A. Hussein
rasha.lasereng@gmail.com

[1] Department of Engineering Applications of Lasers, National Institute of Laser Enhanced Sciences, Cairo University, Giza, Egypt

[2] Department of Physics, Faculty of Science, Al-Muthana University, Muthana, Iraq

[3] Centre for Photonics and Smart Materials, Zewail City of Science and Technology, Sheikh Zayed District, 6th of October City, Giza, Egypt

[4] Faculty of Engineering, Mathematics and Engineering Physics Department, Mansoura University, Mansoura, Egypt

1 Introduction

Photonic crystal fibers (PCFs) are widely investigated in optical fiber devices and sensors (Wang et al. 2011). PCF is a microstructured fiber consisting of air hole arrays running along the entire length of the fiber. PCFs can be divided into two types according to the guiding mechanism. The first is named index-guiding PCF (Sharma et al. 2013) which is based on the modified total internal reflection (MTIR). However, the second kind of PCFs is known as photonic bandgap (PBG) fiber (Cregan et al. 1999) which allows the light propagation in a low-index core. PCF has unique properties that are not available in standard optical fibers, such as endless single-mode operation (Birks et al. 1997), large mode area (Napierała et al. 2010), and tailorable chromatic dispersion (Shi et al. 2011). The waveguiding properties of PCF can also be controlled easily by varying geometrical parameters. In addition, the PCF air-holes can be infiltrated by different materials such as ethanol (Yiou et al. 2005), polymers (Huan et al. 2004), and liquid crystal (LC) (Hameed et al. 2011a; Hameed and Obayya 2014). The LC is of particular interest since its refractive index can be tuned either thermally or electrically (Ren et al. 2008).

High birefringence is one of the unique properties of PCF, therefore many research projects are focused on this property. Birefringent PCF (Ren et al. 2008; Hansen et al. 2001; Chen and Shen 2007; Hameed et al. 2009, 2011b) can be realized by breaking down the fiber's structure symmetry either by changing structure parameters or by air-hole infiltration with different materials. In (Hansen et al. 2001), the authors used an asymmetric core PCF, with highly regular triangular lattice. They obtained a birefringence of 9.3×10^{-4} at the operating wavelength $\lambda = 1.55$ μm. In addition, Chen and Shen (2007) have obtained high birefringence larger than 0.01 by using PCF with circular and elliptical air holes in the cladding and core regions, respectively. The LC is a birefringent material due to the difference between its ordinary n_o and extraordinary n_e refractive indices. In 2008, Ren et al. (2008) have presented LC PBG fiber with high birefringence of 0.02. Additionally, Hameed et al. (2011b) have reported soft glass PCF with small LC core with high birefringence of 0.042 at the operating wavelength $\lambda = 1.55$ μm.

In this paper, highly birefringent nematic LC PCF (NLC–PCF) is presented and investigated. The simulation is obtained by using full vectorial finite element method (FVFEM) (Zhang and Xu 1995; Obayya 2011) with arbitrary permittivity tensor and perfectly matched layer boundary condition. The suggested design depends on using silica glass and E7 nematic LC (NLC) core. Since the ordinary n_o and extraordinary n_e refractive indices of the E7 material are higher than the refractive index of the silica n_s, the propagation through the NLC–PCF occurs by MTIR. In addition, the NLC infiltration (Hameed et al. 2009, 2011b; Haakestad et al. 2005; Hu et al. 2012) increases the birefringence between the two fundamental guided modes. As n_o and n_e of the NLC can be tuned either thermally or electrically, the presented design offers tunability with temperature and external electric field. This tunability makes the suggested design applicable in optical communication and biosensing. The suggested triangular lattice silica NLC–PCF can be realized by stack and draw method (Knight et al. 1996). Additionally, Huan et al. (2004) demonstrated selective filling method in which only the central hole is filled. In Gibson et al. (2005), the authors have manufactured a nano-structured holes in photonic crystal fiber with hole pitch of $\Lambda \sim 120$ nm, hole diameter ~ 60 nm, and with core size of <100 nm. Therefore, the authors believe that the proposed design can be experimentally achieved. In this investigation, the effects of design parameters, temperature, tilt angle Θ, and twist angle φ on the performance of the suggested design are studied in detail.

2 Numerical method

Starting from Maxwell's equations, the following vector wave equation of the magnetic field can be obtained

$$\nabla \times (\varepsilon^{-1} \nabla \times \mathrm{H}) - \omega^2 \mu_o \mathrm{H} = 0 \tag{1}$$

where ω is the angular frequency, μ_o is the free space permeability, and ε is the permittivity tensor of the waveguide material given by:

$$\varepsilon = \varepsilon_o \varepsilon_r = \varepsilon_o \begin{pmatrix} \varepsilon_{xx} & \varepsilon_{xy} & \varepsilon_{xz} \\ \varepsilon_{yx} & \varepsilon_{yy} & \varepsilon_{yz} \\ \varepsilon_{zx} & \varepsilon_{zy} & \varepsilon_{zz} \end{pmatrix} \tag{2}$$

where ε_o is the free space permittivity and ε_r is the relative permittivity of the waveguide material. The cross section of the waveguide structure is discretized using vector finite element method (VFEM) (Zhang and Xu 1995; Obayya 2011). Applying the standard finite element method (FEM) procedure to the vector wave equation, the following eigenvalue equation can be derived:

$$[\mathrm{K}]\{\mathrm{H}\} - \beta^2 [\mathrm{M}]\{\mathrm{H}\} = \{0\} \tag{3}$$

where [K] and [M] are the global stiffness and mass matrices, {H} is the global magnetic field vector, {0} is the null vector and β *is* the propagation constant. The eigenvalue equation can be solved to obtain the eigenvector **H**, and the corresponding eigenvalue β. Additionally, the effective index of the propagating mode is calculated from β since $n_{eff} = \beta/k$, where k is the free space wave number.

In this study, the computational window is equal to 21 μm × 19 μm and the fiber cross section is divided into 17,170 triangular elements, with 120,403 degrees of freedom for the employed elements. Through the modal analysis, a set of modes is calculated by the FVFEM (Zhang and Xu 1995; Obayya 2011), and the dominant mode is defined as the mode with the highest real effective index value. Since $\nabla \cdot \mathrm{H} = 0$ and interface boundary conditions are automatically satisfied in the formulation, then there is no chance for spurious (nonphysical) modes to appear in the spectrum of the solution.

3 Design and numerical results

Figure 1 shows schematic diagram of the proposed highly birefringent NLC–PCF. All the cladding air holes have the same diameter d and are arranged with hole pitch $\Lambda = 2.9$ μm and d/Λ ratio = 0.8. The big central hole has a diameter $d_o = 3.4$ μm and is infiltrated with E7 NLC material. The suggested PCF is index guiding, and can be placed between two electrodes (Haakestad et al. 2005) to control the orientation of the NLC director (Pitilakis et al. 2011). Depending on the applied voltage the NLC molecules can be tilted or twisted. In addition, n_o, n_e refractive indices of the E7 material are calculated using the following Cauchy model (Li et al. 2005).

$$n_o = A_o + \frac{B_o}{\lambda^2} + \frac{C_o}{\lambda^4} \tag{4}$$

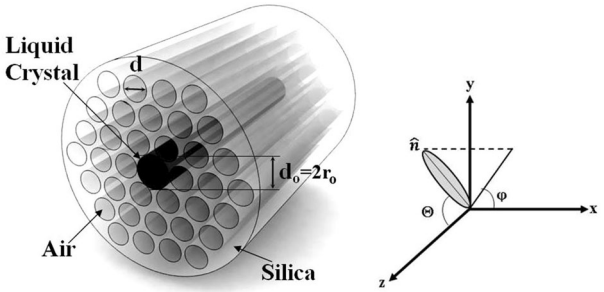

Fig. 1 The structure of the suggested NLC–PCF. The tilt Θ and twist φ angle definitions for NLC director are shown at the *right*

$$n_e = A_e + \frac{B_e}{\lambda^2} + \frac{C_e}{\lambda^4} \tag{5}$$

where A_o, B_o, C_o, A_e, B_e, and C_e are the coefficients of the Cauchy model. These coefficient can be found in (Li et al. 2005) at different temperatures. The relative permittivity tensor (Hsu et al. 2008) of the NLC is calculated as follows

$$\begin{aligned}
\varepsilon_{xx} &= n_o^2 + (n_e^2 - n_o^2)\sin^2\Theta\cos^2\varphi \\
\varepsilon_{xy} &= \varepsilon_{yx} = (n_e^2 - n_o^2)\sin^2\Theta\sin\varphi\cos\varphi \\
\varepsilon_{xz} &= \varepsilon_{zx} = (n_e^2 - n_o^2)\sin\Theta\cos\Theta\cos\varphi \\
\varepsilon_{yy} &= n_o^2 + (n_e^2 - n_o^2)\sin^2\Theta\sin^2\varphi \\
\varepsilon_{yz} &= \varepsilon_{zy} = (n_e^2 - n_o^2)\sin\Theta\cos\Theta\sin\varphi \\
\varepsilon_{zz} &= n_o^2 + (n_e^2 - n_o^2)\cos^2\Theta
\end{aligned} \tag{6}$$

where Θ is the tilt angle between the NLC director $\hat{n}$ and the z-axis as shown in Fig. 1. However, φ is the twist angle between the projection of crystal director on x–y plane and the x-axis (Chen et al. 2009). The orientation of NLC molecules can be altered by the applied field. The response of the NLC director axis to the applied field depends on the dielectric anisotropy. Furthermore, n_o and n_e of the E7 material are fixed to 1.5024 and 1.6970, respectively at the operating wavelength $\lambda = 1.55$ μm and at temperature T = 25 °C. The n_s of Silica equals to 1.45 at the same wavelength. The birefringence can be defined as

$$B = |n_{effTE} - n_{effTM}| \tag{7}$$

where n_{effTE} and n_{effTM} are the effective indices of the quasi transverse electric (TE) and quasi transverse magnetic (TM) modes, respectively.

3.1 Temperature effect

The performance of the suggested design is affected by the temperature, since the effective indices of the E7 material are temperature dependent. The n_e of the E7 NLC decreases from 1.7096 to 1.6438 at the operating wavelength $\lambda = 1.55$ μm as the temperature T increases from 15 to 50 °C. On the other hand, as T increases from 15 to 35 °C, there is a slight

decrease in n_o from 1.5034 to 1.5017 at the 1.55 μm operating wavelength. When T increases from 35 to 50 °C, the n_o increases from 1.5017 to 1.5089 at the same wavelength. In this study, the fundamental quasi TE mode refers to the fundamental H_{11}^y or E_{11}^x modes, while the fundamental quasi TM mode refers to the fundamental H_{11}^x or E_{11}^y modes according to the Cartesian coordinate shown in Fig. 1. The variation of the effective indices of the quasi TE and quasi TM guided modes with the wavelength at different temperatures is examined as depicted in Fig. 2. During this study the other parameters are fixed to $\Lambda = 2.9$ μm, $d/\Lambda = 0.8$, NLC core radius $r_o = 1.7$ μm, $\varphi = 90°$, and $\Theta = 60°$. At $\varphi = 90°$, and $\Theta = 60°$, ε_{xx} of the permittivity tensor is equal to n_o^2, therefore it is nearly invariant with temperature variation. However, ε_{yy} is affected by the dominant n_e^2, and hence it decreases with increasing temperature. As a result, the effective index of the quasi TM mode decreases as the temperature increases. On the other hand, there is no temperature effect on the quasi TE mode at $\varphi = 90°$, and $\Theta = 60°$. This implies that the birefringence of the reported design decreases with increasing the temperature from 15 to 35 °C as shown in Fig. 3. Figure 3 presents the wavelength dependence of the birefringence for different temperatures from 15 to 35 °C with a 5 °C step. It is noted that the suggested design offers high birefringence of 0.1556 at a wavelength of 1.55 μm and T = 15 °C. Also at T = 25 °C, the birefringence is equal to 0.1466 at the same wavelength. On the other hand, at $\varphi = 0°$, and $\Theta = 60°$, ε_{yy} of the permittivity tensor equals to n_o^2 and hence it is almost

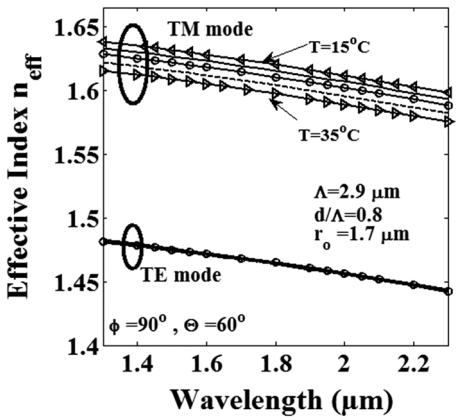

Fig. 2 Variation of the n_{eff} of the quasi TE and quasi TM modes with the wavelength at different temperatures from 15 to 35 °C with a step of 5 °C

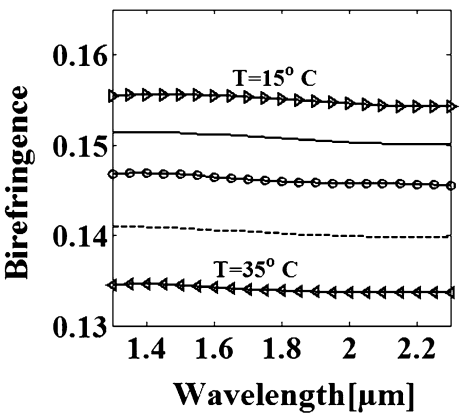

Fig. 3 Variation of the birefringence with the wavelength at different temperatures, from 15 to 35 °C with a step of 5 °C

constant and is not affected by the variation of the temperature. However, ε_{xx} is affected by the dominant n_e^2 and hence is affected by the temperature. Thus, the birefringence variation with temperature at $\varphi = 0°$ results from the change of n_{eff} of the quasi TE mode only. It should be noted that, ε_{xx} and ε_{yy} depend on n_e and n_o, respectively through the range of φ from 0° to 45°. In addition, when φ is in the range from 45° to 90°, ε_{xx} relies on n_o while ε_{yy} depends on the dominant n_e. Therefore, ε_{xx} is almost constant, while ε_{yy} is affected by the variation of the temperature. Hence, the birefringence variation is due to the change of the quasi TM mode effective index in the range $45° \leq \varphi \leq 90°$.

3.2 Tilt angle effect

As previously mentioned, the NLC material can be tilted and twisted depending on the applied voltage. The effect of the tilt angle Θ on the birefringence, A_{eff}, and n_{eff} of the quasi TE and quasi TM modes is studied. The structure parameters used in this investigation are fixed to $\Lambda = 2.9$ μm, d/Λ ratio = 0.8, NLC core radius $r_o = 1.7$ μm, $\varphi = 90°$ and T = 25 °C. It is noted that at $\Theta = 0°$, the effective index of the quasi TM modes is equal to that of the quasi TE mode since $\varepsilon_{xx} = \varepsilon_{yy} = n_o^2$. It is also found that the effective indices of the quasi TM mode at $\varphi = 90°$ increases with increasing the tilt angle Θ while the effective index of the quasi TE mode is nearly constant. Since at $\varphi = 90°$, ε_{xx} of the permittivity tensor equals to n_o^2 for any value of Θ. However, ε_{yy} increases with increasing the angle Θ. Consequently, only the effective index of the quasi TM mode is affected by the tilt angle variation as depicted in Fig. 4. Therefore, the birefringence of the proposed design increases with increasing the tilt angle as shown in Fig. 5.

Figure 5 shows the variation of the birefringence with the wavelength at different tilt angles 0°, 30°, 45°, 60°, and 90°. The reported design offers high birefringence of 0.101, and 0.1911 at $\Theta = 45°$, and 90°, respectively at the operating wavelength $\lambda = 1.55$ μm. As discussed previously, the effective index of the quasi TE mode is nearly invariant for different values of Θ at $\varphi = 90°$. For Θ in the range from 0° to <45°, ε_{yy} comparatively relies on n_o^2, while it is more dependent on n_e^2 in the Θ range from 45° to 90°. Therefore, the core region's effective refractive index and hence the effective index of the quasi TM mode in the range of Θ from 45° to 90° is greater than that in the range from 0° to <45° as shown in Fig. 4. Furthermore, the index contrast seen by the quasi TM mode in the range from 0° to <45° is smaller than that seen in the range from 45° to 90°. As Θ increased from

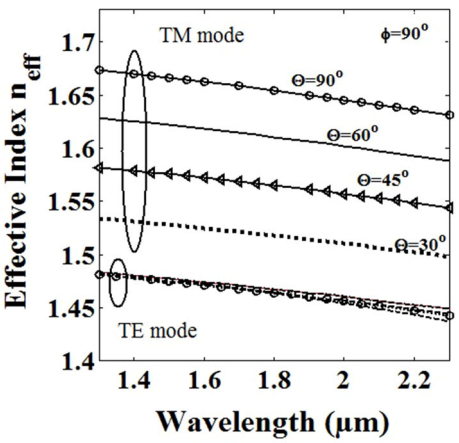

Fig. 4 Variation of the n_{eff} of the quasi TE and TM modes with the wavelength at different tilt angles Θ of the NLC director, 0°, 30°, 45°, 60°, and 90°

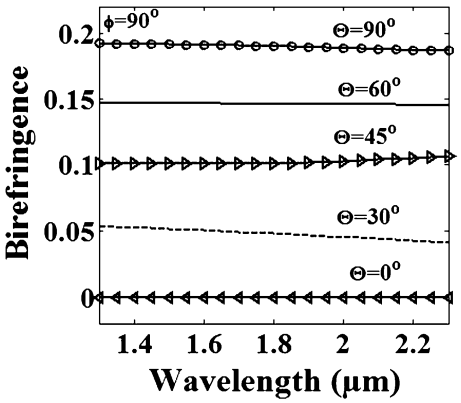

Fig. 5 Variation of the birefringence with the wavelength at different tilt angles Θ of the NLC director, 0°, 30°, 45°, 60°, and 90°

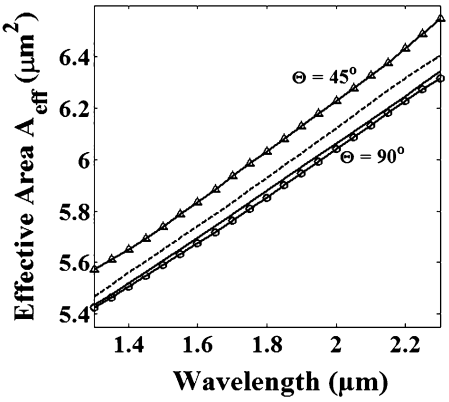

Fig. 6 Variation of the A_{eff} of the quasi TM mode with the wavelength at different tilt angles Θ of the NLC director, from 45° to 90° with a step of 15°

45° to 90°, the index contrast between the core and cladding region is increased. Therefore, the confinement through the core region increases. Consequently, the A_{eff} of the quasi TM mode decreases by increasing Θ as shown in Fig. 5. For example, at $\Theta = 45°$, and 90°, the A_{eff} equals to 5.787, and 5.633 μm^2, respectively at the operating wavelength $\lambda = 1.55$ μm as shown in Fig. 6.

The NLC orientation in the PCF can be implemented by the creation of an additional orienting layer on the inner surface of the air hole of the LC-PCF. The alignment type depends basically on the anchoring conditions, LC structure, and aligning material. However, the orientational configuration of the LC is determined by balancing the elastic forces and anchoring condition. In order to set the alignment direction, the PCF capillaries with the aligning layers on their inner walls should be exposed to polarized light. The alignment layer could be diazodyes (Chigrinov et al. 2002), or commercially available polyimides SE1211 and SE130 (Chychłowski et al. 2011). In Chychłowski et al. (2011), the authors have investigated experimentally the use of orienting layer to control and improve the quality of the LC molecules orientation inside PCF capillaries. In this regard, they have applied two indirect orientation methods within the capillaries: the photo-orientation and temperature induced orientation. On the other hand, these methods require utilization of an additional layer of polyimide to induce an orienting layer. Moreover, the authors have achieved both planar and transverse LC orientation by means of the photo-orienting method (Chychłowski et al. 2010, 2011). However, the escaped radial (splay)

orientation is obtained by temperature-induced alignment which creates homeotropic boundary condition. It should also be noted that, the control of the twist and tilt angles can be achieved as described by Chen et al. (2009) and Huang (2011).

At $\Theta = 90°$, the full permittivity tensor of the E7 NLC is transferred to transverse tensor as follows

$$\varepsilon_r = \begin{pmatrix} n_o^2 + \Delta\varepsilon \cos^2 \varphi & \Delta\varepsilon \sin \varphi \cos \varphi & 0 \\ \Delta\varepsilon \sin \varphi \cos \varphi & n_o^2 + \Delta\varepsilon \sin^2 \varphi & 0 \\ 0 & 0 & n_o^2 \end{pmatrix} \quad (8)$$

where $\Delta\varepsilon = (n_e^2 - n_o^2)$.

The effect of structure parameters on the effective indices of the guided modes, birefringence, and A_{eff} is next discussed. Throughout the following calculations the tilt angle Θ is fixed to 90°.

3.3 Structure parameters effect

The effect of the design parameters on the modal properties of the proposed design is considered at $\Theta = 90°$. The effect of the hole pitch Λ is studied first. In this investigation the d/Λ ratio, NLC core radius r_o, temperature T, tilt angle, and twist angle are fixed to 0.8, 1.7 μm, 25 °C, 90°, and 90°, respectively. In addition the n_s of silica material, n_o, and n_e of the E7 material are fixed to 1.45, 1.5024, and 1.6970, respectively. Figure 7 represents the dependence of the birefringence on the wavelength at different hole pitches. It is evident from this figure that the birefringence decreases by increasing the hole pitch. The birefringence at the operating wavelength $\lambda = 1.55$ μm, is equal to 0.1911 at hole pitch of 2.9 μm which is greater than the high birefringence of 0.042 of a soft glass PCF with small LC core (Hameed et al. 2011b).

Figure 8 displays the variation of the effective indices of the two guided modes with the wavelength at different hole pitches. From this figure, one can reveal that the effective indices of the quasi TE and quasi TM modes are slightly affected by the hole pitch since these modes are well confined and propagated inside the NLC infiltrated core.

The effect of the NLC core radius r_o, on the birefringence of the suggested PCF is presented in Fig. 9. In this evaluation, the hole pitch, d/Λ ratio, twist angle, and temperature are fixed to 2.9 μm, 0.8, 90°, and 25 °C, respectively. It is noted that as the core radius increases, the birefringence also increases. As the core radius increases, the amount

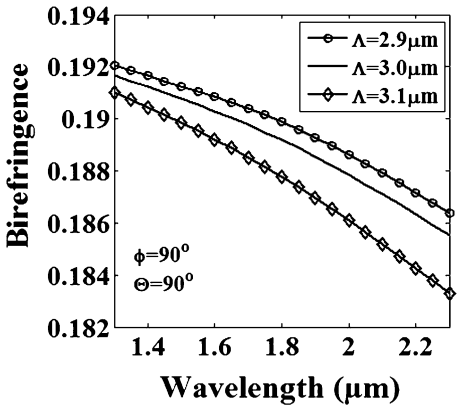

Fig. 7 The wavelength dependent birefringence at different hole pitches 2.9, 3.0, and 3.1 μm

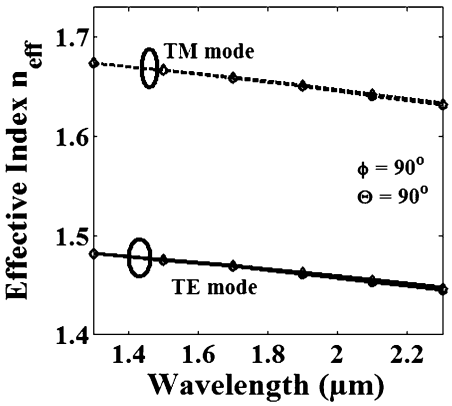

Fig. 8 Variation of the n_{eff} of the two polarized modes with the wavelength at different hole pitches 2.9, 3.0, and 3.1 μm

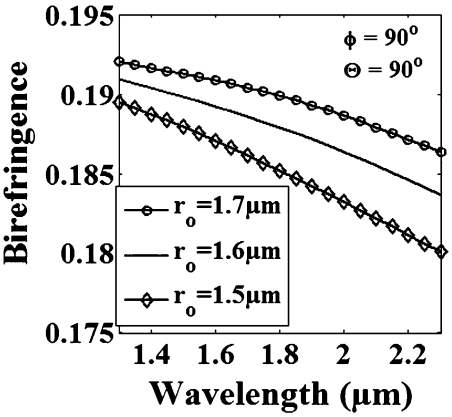

Fig. 9 Variation of the birefringence with the wavelength at different core radii, r_o = 1.7, 1.6, and 1.5 μm

of the NLC infiltration increases. Consequently, the asymmetry of the structure and hence the birefringence increase. At NLC core radius r_o = 1.5, 1.6 and 1.7 μm the birefringence equals to 0.1875, 0.1895, and 0.1911, respectively at the operating wavelength λ = 1.55 μm.

Figure 10 presents the wavelength dependence of the birefringence for three different d/Λ ratios. In this study, the hole pitch, core radius, twist angle, and the temperature are fixed to 2.9, 1.7 μm, 90°, and 25 °C, respectively. As the d/Λ ratio increases, the effective refractive index of the cladding region decreases. Therefore, the index contrast between the core and cladding regions increases. As a result, the modes will be more confined through the NLC core region. Consequently, the birefringence increases by increasing d/Λ ratio as shown in Fig. 10. However, the A_{eff} of the quasi TM mode decreases by increasing d/Λ ratio as shown in Fig. 11. The proposed design with d/Λ = 0.8 offers high birefringence of 0.1911 at the operating wavelength λ = 1.55 μm.

3.4 Twist angle effect

The effect of the twist angle φ of the director on the birefringence is investigated. Four different values of φ, 0°, 30°, 60°, and 90° are discussed. The hole pitch, d/Λ ratio, core

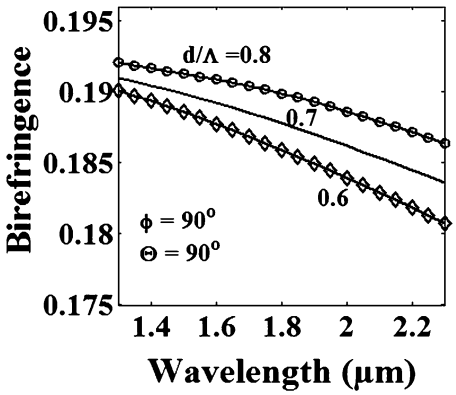

Fig. 10 Variation of the birefringence with the wavelength at different d/Λ ratios, 0.8, 0.7, and 0.6

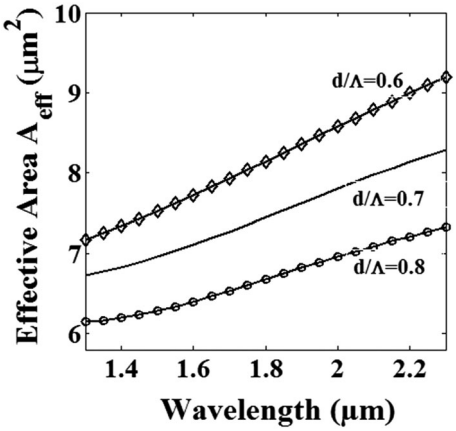

Fig. 11 Variation of A_{eff} of the quasi TM mode with the wavelength at different d/Λ ratios, 0.8, 0.7, and 0.6

radius, and temperature, are fixed to 2.9 μm, 0.8, 1.7 μm, and 25 °C, respectively. It is found that at the range of φ from 0° to <45°, the effective index of the quasi TE mode is greater than that of the quasi TM mode. When φ is in the range from 0° to <45°, ε_{xx} depends on n_e^2 while ε_{yy} relies on n_o^2. However, when φ is in the range from 45° to 90°, ε_{xx} is more dependent on n_o^2 while ε_{yy} is dependent on n_e^2. Figure 12 shows that the difference between the effective indices of the quasi TE and quasi TM modes in the range of φ from 45° to 90° is equal to that in the range of 0° to <45° but with opposite sign. At $\varphi = 90°$, the permittivity tensor ε_r is diagonal of [n_o^2, n_e^2, n_o^2], while at $\varphi = 0°$, ε_r is a diagonal of [n_e^2, n_o^2, n_o^2]. It is evident that ε_{yy} at $\varphi = 90°$ equals to ε_{xx} at $\varphi = 0°$. Hence, the effective index of the quasi TM mode at $\varphi = 90°$ is equal to that of the quasi TE mode at $\varphi = 0°$. Therefore, the differences between these indices are equal but with opposite sign.

One of the important parameters in the design and operation of many optical devices (Rajarajan et al. 2000; Somasiri et al. 2002; Hameed and Obayya 2010) is the modal hybridness. The modal hybridness (Somasiri et al. 2002; Hameed et al. 2010) may be defined as the ratio of the maximum values of the minor to the major fields components. For the quasi TM mode the major field is H_x while the minor field is H_y, and hence the hybridness is equal to H_y/H_x. However, the hybridness of the quasi TE mode is equal to H_x/H_y.

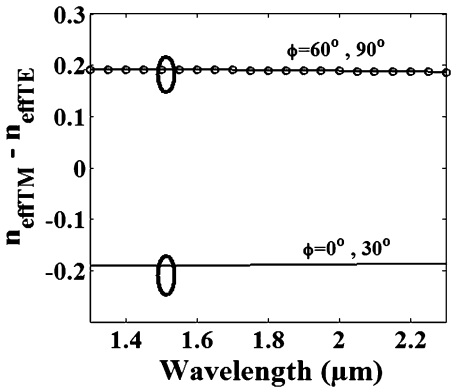

Fig. 12 Variation of the birefringence with the wavelength at different twist angles

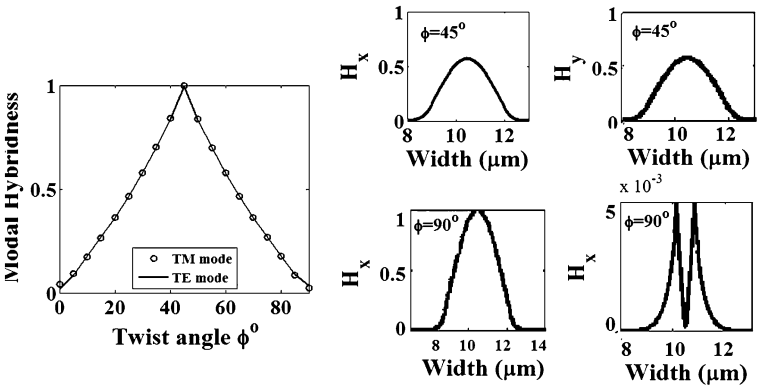

Fig. 13 Variation of the modal hybridness of the two polarized modes with the twist angle at the operating wavelength $\lambda = 1.55$ μm

The variation of the modal hybridness of the two polarized modes with the twist angle φ is depicted in Fig. 13. Throughout this study, the operating wavelength λ, hole pitch Λ, d/Λ ratio, core radius r_o, and Θ are fixed to 1.55, 2.9 μm, 0.8, 1.7 μm, and 90°, respectively. From this figure, one can reveal that the modal hybridness increases with increasing φ in the range from 0° to 45°, while it decreases with increasing φ from 45° to 90°. The hybridness equals to 0.0206 and 0.0349 at $\varphi = 0°$ and 90°, respectively. The reported design offers high hybridness of 0.9999 and 0.9954 for the quasi TM and quasi TE modes, respectively at $\varphi = 45°$. This is confirmed by the field plot of the quasi TM and quasi TE modes at the central line of the NLC–PCF at $\varphi = 45°$ and 90° shown in Fig. 13.

The dependence of modal hybridness on the tilt angle Θ of the NLC director is investigated at two different twist angles $\varphi = 45°$ and 90° as shown in Fig. 14. It is evident from Fig. 14a that at $\varphi = 45°$ and at $\Theta = 0°$, $\varepsilon_r = [n_o^2, n_o^2, n_e^2]$ and the modal hybridness is very low. In addition, ε_r is independent on the twist angle φ. As Θ is increased over 10°, the modal hybridness is nearly constant at unity. Moreover, the modal hybridness of the quasi TE and quasi TM modes are approximately equal. On the other hand, at $\varphi = 90°$ the quasi TE mode has more hybridness than the quasi TM mode as shown in Fig. 14b.

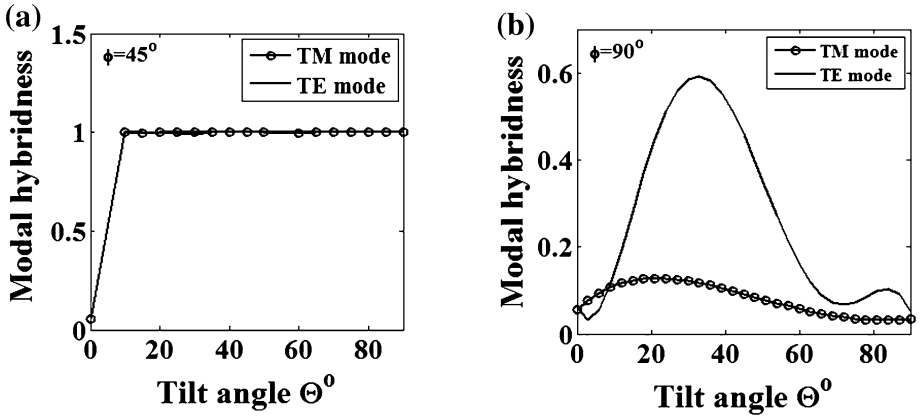

Fig. 14 Variation of the modal hybridness of the two polarized modes with the tilt angle at the operating wavelength $\lambda = 1.55$ μm at **a** $\varphi = 45°$, **b** $\varphi = 90°$

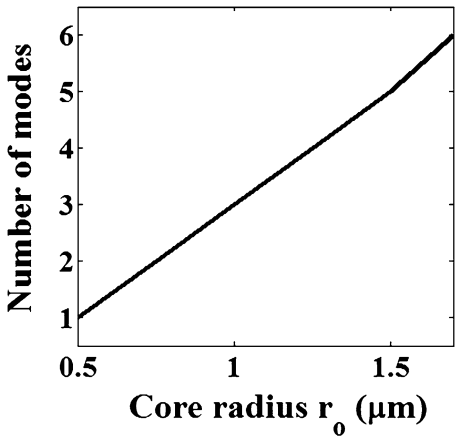

Fig. 15 Variation of number of modes with the core radius at the operating wavelength $\lambda = 1.55$ μm

The effect of the NLC core radius on the number of modes is also investigated as shown in Fig. 15. It is revealed from this figure that the number of supported modes increase with increasing the central NLC radius. Additionally, the proposed design supports only the fundamental modes when the NLC core radius is equal to $r_o = 0.5$ μm with birefringence of 0.08. In order to increase the birefringence at NLC core radius $r_o = 0.5$ μm, the other geometrical parameters can be optimized. The numerical results show that the birefringence at NLC core radius $r_o = 0.5$ μm is increased to 0.1143 at the operating wavelength $\lambda = 1.55$ μm as shown in Fig. 16. In this study, the hole pitch, d/Λ ratio, core radius, rotation angle, and temperature are fixed to $\Lambda = 2.7$ μm, $d/\Lambda = 0.6$, $r_o = 0.5$ μm, $\varphi = 90°$, and $T = 25$ °C, respectively. Further, the structure is squeezed in y direction so that the distance between holes in y-direction is equal to $(\sqrt{3}/4)\,\Lambda$.

The effect of the number of rings of the microstructured cladding on the confinement losses of the proposed design have been investigated. It is found that the confinement loss

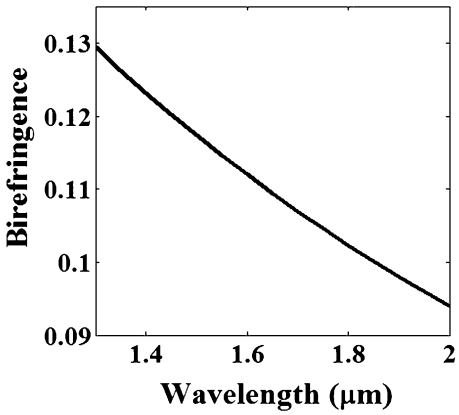

Fig. 16 Variation of the birefringence with the wavelength at $\Lambda = 2.7$ μm, $d/\Lambda = 0.6$, $r_o = 0.5$ μm, and $\varphi = 90°$

have decreased from 3.721×10^{-5} to 3.692×10^{-11} dB/m by increasing the number of rings from one ring to three rings only, respectively.

It is worth noting that, the scattering losses and absorption of the NLC material are much greater than that of the background material such as silica, FK51A, and Pyrex (Alkeskjold et al. 2004). Consequently, the loss of background material can be neglected. Besides that, Hu and Whinnery (1974) have reported that the scattering loss of the bulk NLC is between 15 and 40 dB/cm which is much larger than its absorption losses at the visible and near-infrared wavelengths. However, the scattering loss of the NLCs can be decreased from 3.25 to 1.3 dB/cm by filling the capillaries with diameters of 4 and 5.1 μm, respectively with LC materials as reported by Green and Madden (1989). In this study (Green and Madden 1989), the authors have used Pyrex fiber having refractive index of 1.47 with a core diameter of 4 μm. The capillary rise method has been used to fill the fiber with an E47 mixtures whose director was along the fiber axis. In addition, the scattering losses of silica fiber filled with NLC have been analyzed (Green and Madden 1989) scattering losses from 1.5 to 2.4 dB/cm have been obtained for estimated insertion efficiencies of 0.2–100 % using fiber length of 30 cm. The authors (Green and Madden 1989) have revealed that the scattering loss is affected by the filling technique.

4 Conclusion

An index guiding NLC–PCF with high birefringence is proposed and analyzed using FVFEM. The reported design has a silica background material with a large central hole filled with an E7 NLC material. High birefringence of 0.191 is achieved at the operating wavelength $\lambda = 1.55$ μm when the NLC diameter is equal to 3.4 μm at temperature $T = 25$ °C, $\Theta = 90°$ and $\varphi = 90°$. In addition, the birefringence can be increased to 0.2025 by decreasing the temperature to 15 °C. Moreover, high birefringence of 0.08 is obtained with single mode NLC–PCF at $\lambda = 1.55$ μm and NLC core diameter of 1.0 μm.

Ethical standard The authors would like to ensure the objectivity and transparency in the submitted research paper. Additionally, the authors would like to ensure that accepted principles of ethical and professional conduct have been followed through the preparation of the proposed paper. Further, we would like to clarify that there is no sources of funding, and no potential conflicts of interest (financial or non-financial). Moreover, the submitter research does not involve human participants, or animals.

References

Alkeskjold, T., Lægsgaard, J., Bjarklev, A., Hermann, D., Anawati, A., Broeng, J., Li, J., Wu, S.: All-optical modulation in dye-doped nematic liquid crystal photonic bandgap fibers. Opt. Express **12**, 5857–5871 (2004)

Birks, T.A., Knight, J.C., Russell, P.: Endlessly single-mode photonic crystal fiber. Opt. Lett. **22**, 961–963 (1997)

Chen D., Shen, L.: Ultrahigh birefringent photonic crystal fiber with ultralow confinement loss. IEEE Photon. Technol. Lett., **19**, 185–187 (2007)

Chen, MY., Chang, H.C.: Finite-difference frequency-domain analysis of nematic liquid crystal optical waveguides in silicon V-grooves. CLEO/Pacific RIM'09, (2009)

Chen, M.Y., Hsu, S.M., Chang, H.C.: A finite-difference frequency-domain method for full-vectorial mode solutions of anisotropic optical waveguides with an arbitrary permittivity tensor. Opt. Express **17**, 5965–5979 (2009)

Chigrinov, V., Prudnikova, E., Kozenkov, V., Kwok, H., Akiyama, H., Kawara, T., Takada, H., Takatsu, H.: Synthesis and properties of azo dye aligning layers for liquid crystal cells. Liq. Cryst. **29**, 1321–1327 (2002)

Chychłowski, M.S., Ertman, S., Tefelska, M.M., Wolinski, T.R., Kruszelnicki, E.N., Yaroshchuk, O.: Photo-induced orientation of nematic liquid crystals in microcapillaries. Acta Phys. Pol. A **118**, 1100–1103 (2010)

Chychlowski, M.S., Nowinowski-Kruszelnicki, E., Woliński, T.R.: Liquid crystal orientation control in photonic liquid crystal fibers. SPIE Proceedings, 7753, (2011)

Cregan, R.F., Mangan, B.J., Knight, J.C., Birks, T.A., Russell, P.S.J., Roberts, P.J., Allan, D.C.: Single-mode photonic band gap guidance of light in air. Science **285**, 1537–1539 (1999)

Gibson, B.C., Huntington, S.T., Rubanov, S., Olivero, P.: Exposure and characterization of nano-structured hole arrays in tapered photonic crystal fibers using a combined FIB/SEM technique. Opt. Express **13**, 9023–9028 (2005)

Green, M., Madden, S.J.: Low loss nematic liquid crystal cored fiber waveguides. Appl. Opt. **28**, 5202–5203 (1989)

Haakestad, M.W., Alkeskjold, T.T., Nielsen, M.D., Scolari, L., Riishede, J., Engan, H.E., Bjarklev, A.: Electrically tunable photonic bandgap guidance in a liquid–crystal-filled photonic crystal fiber. IEEE Photon. Technol. Lett. **17**, 819–821 (2005)

Hameed, M.F.O., Obayya, S.S.A., Al-Begain, K., Abo el Maaty, M.I., Nasr, A.M.: Modal properties of an index guiding nematic liquid crystal based photonic crystal fiber. IEEE J. Lightwave Technol. **27**(21), 4754–4762 (2009)

Hameed, M.F.O., Obayya, S.S.A.: Analysis of polarization rotator based on nematic liquid crystal photonic crystal fiber. J. Lightwave Technol. **28**, 806–815 (2010)

Hameed, M.F.O., Obayya, S.S.A.: Coupling characteristics of dual liquid crystal core soft glass photonic crystal fiber. IEEE J. Quantum Electron. **47**, 1283–1290 (2011)

Hameed, M.F.O., Obayya, S.S.A., El-Mikati, H.A.: Highly nonlinear birefringent soft glass photonic crystal fiber with liquid crystal core. IEEE Photon. Technol. Lett. **23**(20), 1478–1480 (2011)

Hameed, M.F.O., Obayya, S.S.A.: Ultra short silica liquid crystal photonic crystal fiber polarization rotator. Opt. Lett. **39**(4), 1077–1080 (2014)

Hansen, T.P., Broeng, J., Libori, S.E.B., et al.: Highly birefringent index-guiding photonic crystal fibers". IEEE Photon. Technol. Lett. **13**, 588–590 (2001)

Hsu, S., Chang, H.: Characteristic investigation of 2D photonic crystals with full material anisotropy under out-of-plane propagation and liquid-crystal-filled photonic-band-gap-fiber applications using finite element methods. Opt. Express **16**, 21355–21368 (2008)

Hu, C., Whinnery, J.R.: Losses of a nematic liquid-crystal optical waveguide. J. Opt. Soc. Am. **64**, 1424–1432 (1974)

Hu, D.J.J., Lim, J.L., Cui, Y., Milenko, K., Wang, Y., Shum, P.P., Wolinski, T.: Fabrication and characterization of a highly temperature sensitive device based on nematic liquid crystal-filled photonic crystal fiber. IEEE Photon. J. **4**, 1248–1255 (2012)

Huan, Y.G., Xu, Y., Yariv, A.: Fabrication of functional microstructured optical fibers through selective filling technique. Appl. Phys. Lett. **85**, 5182–5184 (2004)

Huang, C.: Solving the full anisotropic liquid crystal waveguides by using an iterative pseudospectral-based eigenvalue method. Opt. Express **19**, 3363–3378 (2011)

Knight, J.C., Birks, T.A., Russell, P.S., Atkin, D.M.: All-silica single-mode optical fiber with photonic crystal cladding. Opt. Lett. **21**, 1547–1549 (1996)

Li, J., Wu, S.T., Brugioni, S., Meucci, R., Faetti, S.: Infrared refractive indices of liquid crystals. J. Appl. Phys. **97**, 073501-1–073501-5 (2005)

Napierała, M., Nasiłowski, T., Pawlik, E., Berghmans, F., Wójcik, J., Thienpont, H.: Extremely large-mode-area photonic crystal fibre with low bending loss. Opt. Express **18**, 15408–15418 (2010)

Obayya, S.S.A.: Computational photonics. Wiley, Lodon (2011)

Pitilakis, A.K., Zografopoulos, D.C., Kriezis, E.E.: In-line polarization controller based on liquid-crystal photonic crystal fibers. IEEE J. Lightwave Technol. **29**, 2560–2569 (2011)

Rajarajan, M., Obayya, S.S.A., Rahman, B.M.A., Grattan, K.T.V., El-Mikati, H.A.: Characterisation of low-loss waveguide bends with offset-optimisation for compact photonic integrated circuits. IEEE Proc. Optoelectron. **147**(6), 382–388 (2000)

Ren, G., Shum, P., Hu, J., Yu, X., Gong, Y.: Study of polarization-dependent bandgap formation in liquid crystal filled photonic crystal fibers. IEEE Photon. Technol. Lett. **20**, 602–604 (2008)

Somasiri, N., Rahman, B.M.A., Obayya, S.S.A.: Fabrication tolerance study of a compact passive polarization rotator. IEEE J. Lightwave Technol. **20**, 751–757 (2002)

Sharma, M., Borogohain, N., Konar, S.: Index guiding photonic crystal fibers with large birefringence and walk-off. IEEE J. Lightwave Technol. **31**, 3339–3344 (2013)

Shi, F., Wu, Y., Li, M., Zhao, Y., Zhao, L.: Highly birefringent two-mode photonic crystal fibers with near-zero flattened dispersion. IEEE Photon. J. **3**, 1181–1188 (2011)

Wang, Y.Y., Yang, M., Wang, D.N.: Selectively infiltrated photonic crystal fiber with ultrahigh temperature sensitivity. IEEE Photon. Technol. Lett. **23**, 1520–1522 (2011)

Yiou, S., Delaye, P., Rouvie, A., Chinaud, J., Frey, R., Roosen, G., Viale, P., F'evrier, S., Roy, P., Auguste, J.L., Blondy, J.M.: Stimulated Raman scattering in an ethanol core microstructured optical fiber. Opt. Express **13**, 4786–4790 (2005)

Zhang, L., Xu, S.: Edge-element analysis of anisotropic waveguides with full permittivity and permeability matrices. Int. J. Infrared Millimeter Waves **16**(8), 1351–1360 (1995)